Kinetic study of azobenzene *E*/*Z* isomerization using ion mobility-mass spectrometry and liquid chromatography-UV detection.

Salomé Poyer[1,2*], Chang Min Choi[3], Claire Deo[4], Nicolas Bogliotti[4], Juan Xie[4], Philippe Dugourd[5], Fabien Chirot[6], Jean-Yves Salpin.[1,2]*

[1] Université Paris-Saclay, Univ Evry, CNRS, LAMBE, Evry-Courcouronnes, 91025, France

[2] CY Cergy Paris Université, CNRS, LAMBE, 95000, Cergy, France

[3] Center for Scientific Instrumentation, Korea Basic Science Institute, Chungbuk, Republic of Korea

[4.] Université Paris-Saclay, ENS Paris-Saclay, CNRS, PPSM, 94235 Cachan, France

[5.] Univ Lyon, Université Claude Bernard Lyon 1, CNRS, UMR5306 Institut Lumière Matière, 69622 Villeurbanne, France

[6.] Univ Lyon, Université Claude Bernard Lyon 1, CNRS, ENS de Lyon, UMR5280 Institut des Sciences Analytiques, 69622 Villeurbanne, France

Supporting information

Complete citation for the Gaussian code of programs

Gaussian 09, Revision C.01,
M. J. Frisch, G. W. Trucks, H. B. Schlegel, G. E. Scuseria, M. A. Robb, J. R. Cheeseman, G. Scalmani, V. Barone, B. Mennucci, G. A. Petersson, H. Nakatsuji, M. Caricato, X. Li, H. P. Hratchian, A. F. Izmaylov, J. Bloino, G. Zheng, J. L. Sonnenberg, M. Hada, M. Ehara, K. Toyota, R. Fukuda, J. Hasegawa, M. Ishida, T. Nakajima, Y. Honda, O. Kitao, H. Nakai, T. Vreven, J. A. Montgomery, Jr., J. E. Peralta, F. Ogliaro, M. Bearpark, J. J. Heyd, E. Brothers, K. N. Kudin, V. N. Staroverov, T. Keith, R. Kobayashi, J. Normand, K. Raghavachari, A. Rendell, J. C. Burant, S. S. Iyengar, J. Tomasi, M. Cossi, N. Rega, J. M. Millam, M. Klene, J. E. Knox, J. B. Cross, V. Bakken, C. Adamo, J. Jaramillo, R. Gomperts, R. E. Stratmann, O. Yazyev, A. J. Austin, R. Cammi, C. Pomelli, J. W. Ochterski, R. L. Martin, K. Morokuma, V. G. Zakrzewski, G. A. Voth, P. Salvador, J. J. Dannenberg, S. Dapprich, A. D. Daniels, O. Farkas, J. B. Foresman, J. V. Ortiz, J. Cioslowski, and D. J. Fox, Gaussian, Inc., Wallingford CT, 2010

Table S1. Nature of the complexes observed with azobenzene under electrospray conditions, in function of the ionizing agent.

Ionizing agent	**Complex generated onto the ESI-MS spectrum**
H^+	$[M+H]^+$, $[2M+H]^+$
Li^+, Na^+, K^+, Rb^+, Cs^+	$[M+Alk]^+$, $[2M+Alk]^+$
Ca^{2+}, Sr^{2+}, Mn^{2+}	$[3M+Cat]^{2+}$, $[4M+Cat]^{2+}$ (M=*Z1*, *Z2*)
Ba^{2+}	$[3M+Ba]^{2+}$(M=E, *Z1*, *Z2*)
	$[4M+Ba]^{2+}$ (M=*Z1*, *Z2*)
	$[5M+Ba]^{2+}$, $[6M+Ba]^{2+}$ (M=*Z1*)
Ag^+, Cu^{2+}	$[M+Cat]^+$, $[2M+Cat]^+$
Ni^{2+}	$[2M+Ni]^{2+}$, $[3M+Ni]^{2+}$, $[4M+Ni]^{2+}$ (M=*Z1*, *Z2*)
Cd^{2+}	$[2M+Cd]^{2+}$, $[3M+Cd]^{2+}$, $[4Z1+Cd]^{2+}$ (M=*Z1*, *Z2*)
Fe^{2+}	$[4Z1+Fe]^{2+}$, $[2(E-58)+Fe]^{2+}$, $[3(Z2-58)+Fe]^{2+}$
Co^{2+}, Zn^{2+}	$[4Z1+Cat]^{2+}$, $[2Z2+Cat]^{2+}$, $[E+Cat]^{2+}$
Fe^{3+}, Ti^{3+}, Au^{3+}, La^{3+}, Eu^{3+}	No complexes

Figure S1. CID MS/MS spectra observed for a) $[Z2+H]^+$, b) $[E+H]^+$ and c) $[Z1+H]^+$.

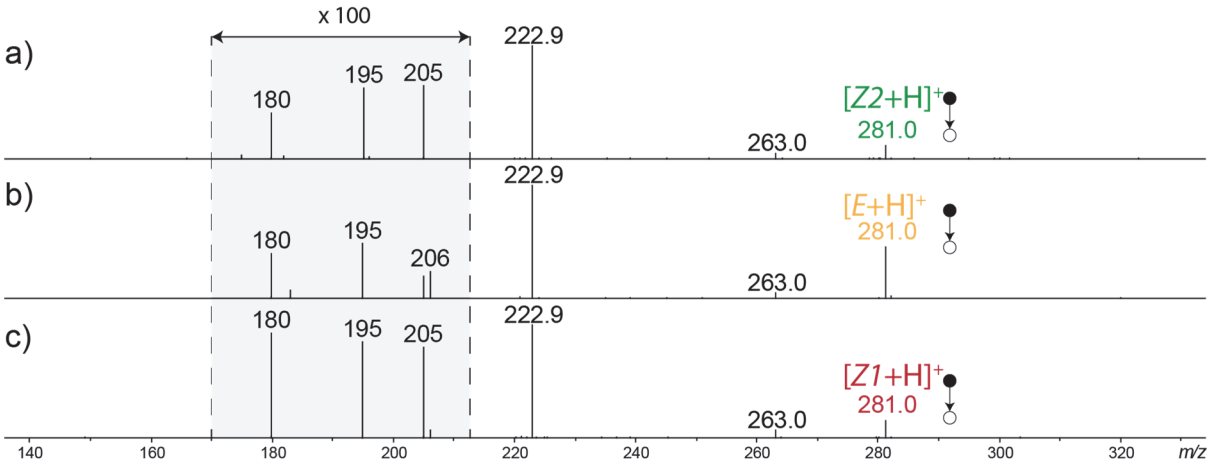

Figure S2. MS spectra observed for a) *Z2*, b) *E* and c) *Z1* after HPLC separation and silver complexation. To generate $[M+Ag]^+$ and $[2M+Ag]^+$ ions, 10 µM of $AgNO_3$ were added to the aqueous mobile phase.

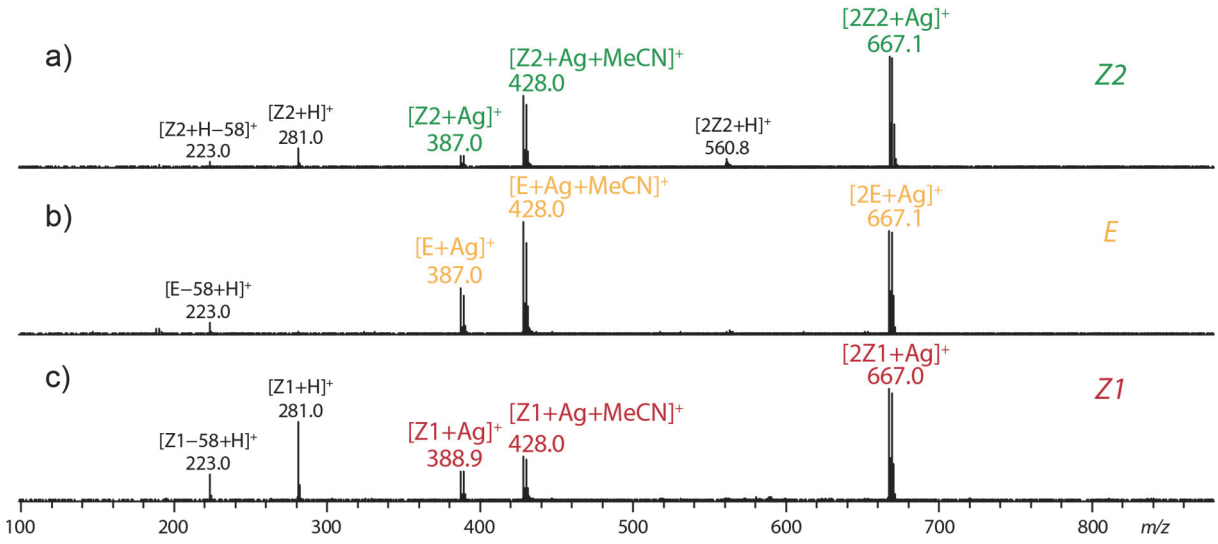

Figure S3. CID MS/MS spectra observed for a) $[Z2+Ag]^+$, b) $[E+Ag]^+$ and c) $[Z1+Ag]^+$.

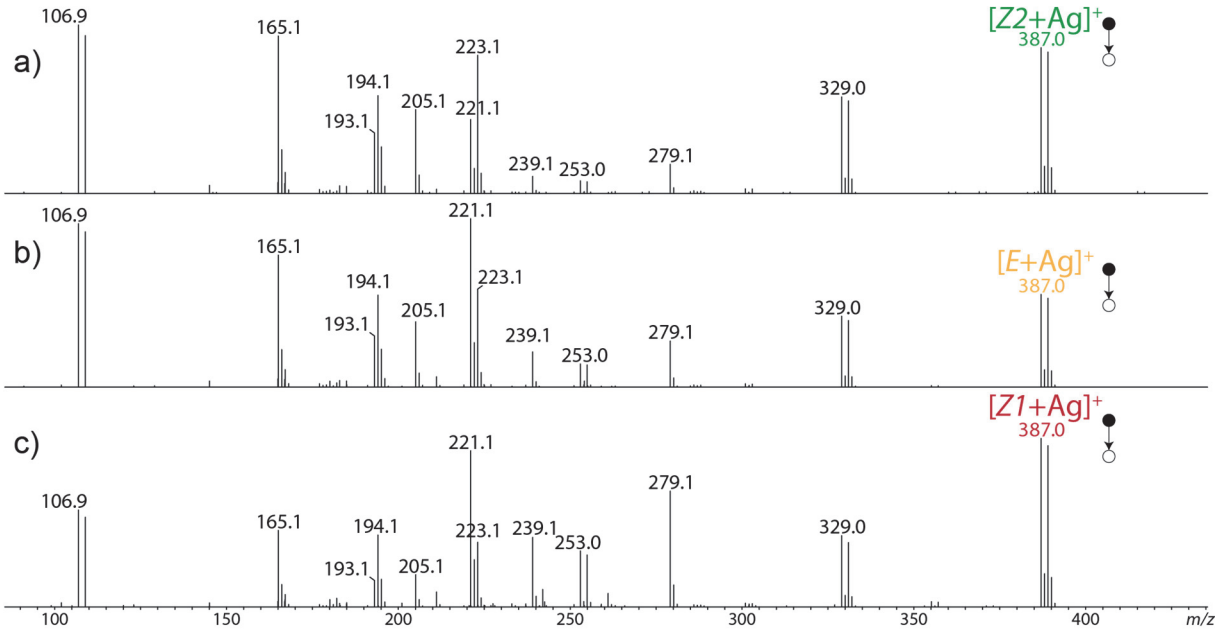

Figure S4. MS spectra observed for a) *Z2*, b) *E* and c) *Z1* after HPLC separation and calcium complexation. To generate $[3Z+Ca]^{2+}$ and $[4Z+Ca]^{2+}$ ions, 10 µM of $CaCl_2$ were added to the aqueous mobile phase.

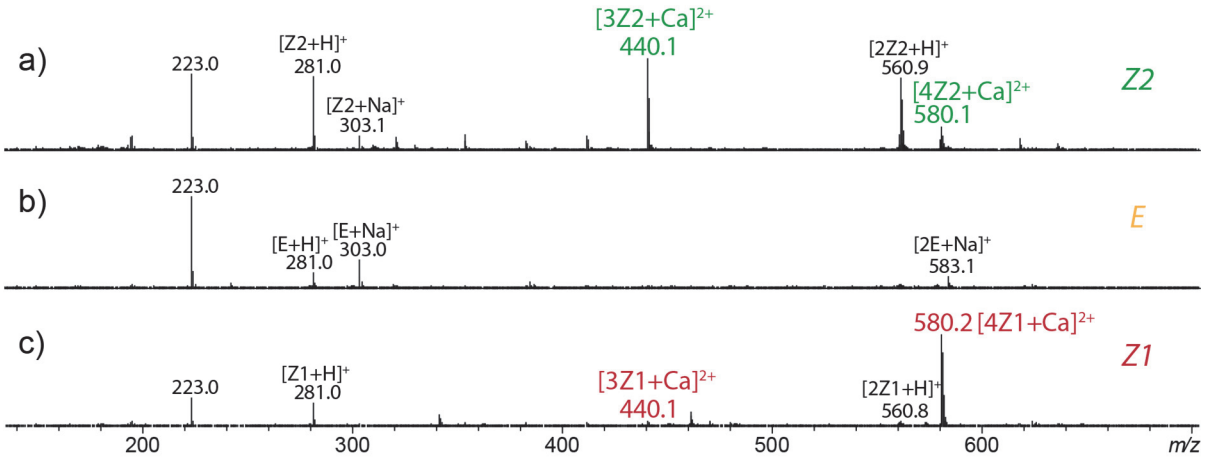

Figure S5. MS spectra observed for a) *Z2*, b) *E* and c) *Z1* after HPLC separation and zinc complexation. To generate Zn complex ions, 100 µM of $ZnSO_4$ were added to the aqueous mobile phase.

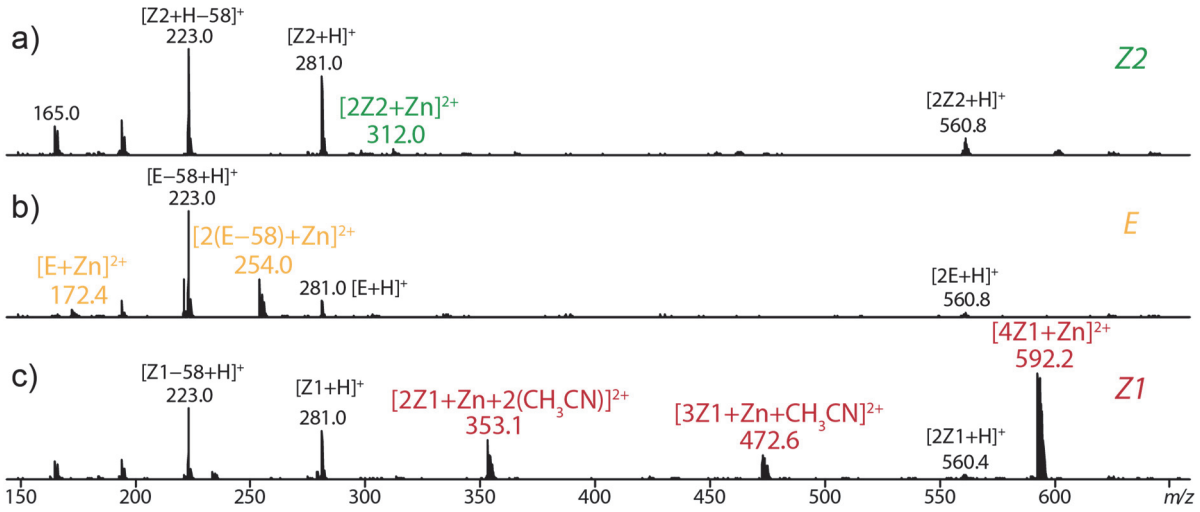

Figure S6. MS spectra observed for a) *Z2*, b) *E* and c) *Z1* after HPLC separation and iron complexation. To generate Fe complex ions, 100 µM of $FeCl_2$ were added to the aqueous mobile phase.

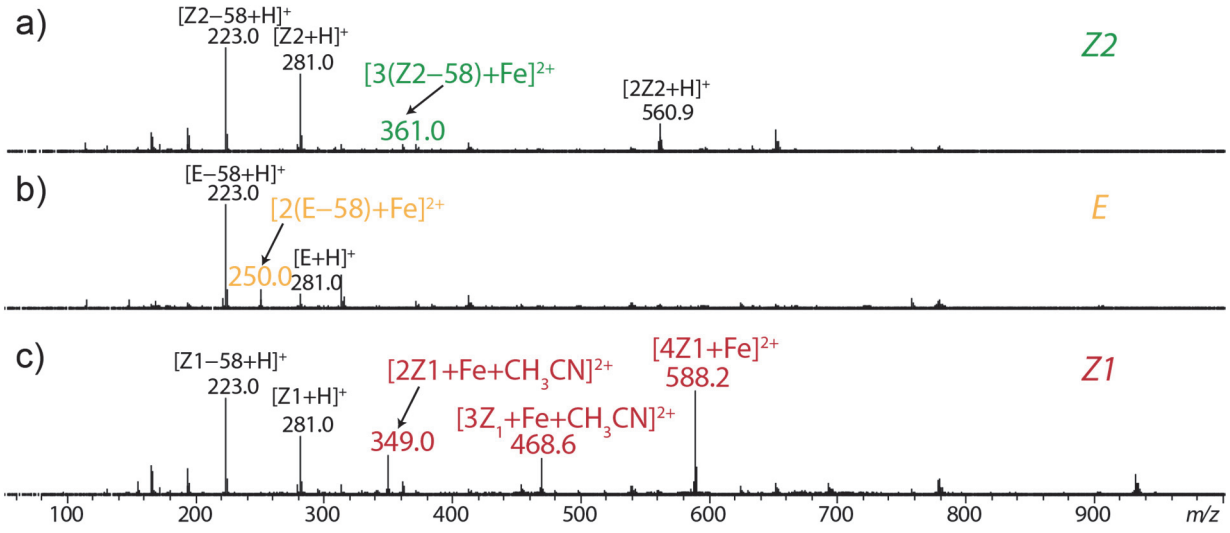

Figure S7. Relative HPLC peak integration area in function of the time used to determine the proportion of *E*→*Z1*/*Z2* isomers from LC-UV coupling for the different solvents at 30°C.

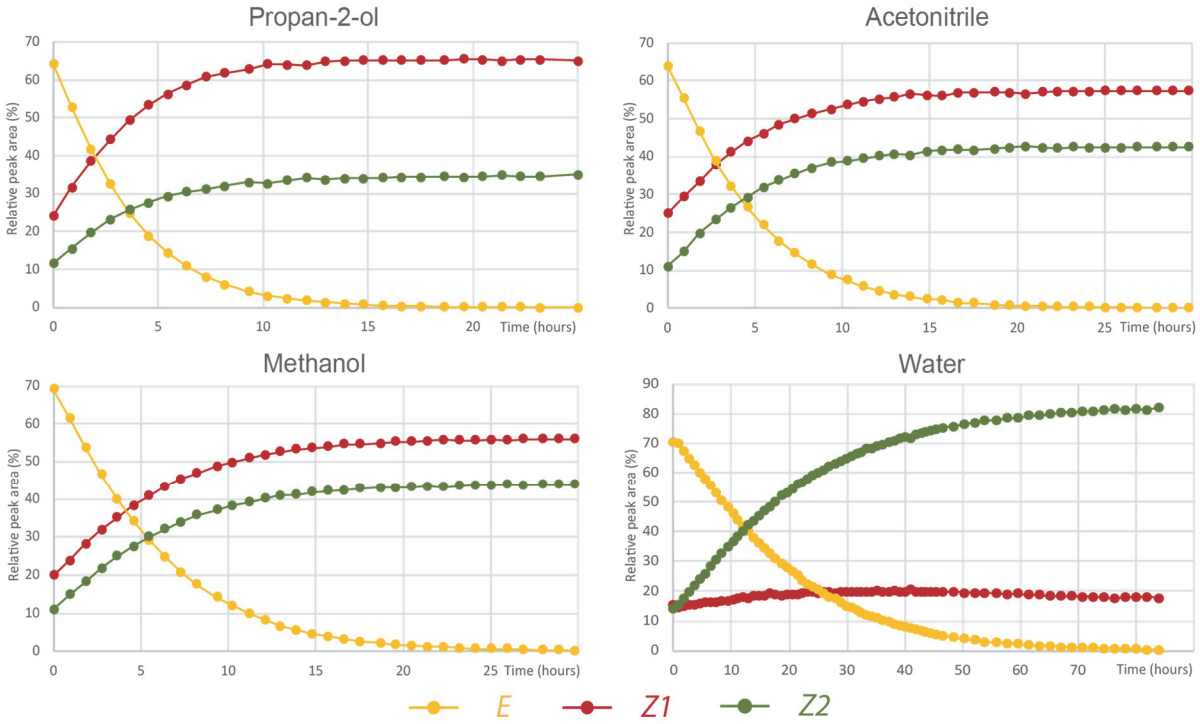

Figure S8. Relative HPLC peak integration area in function of the time used to determine the proportion of *E*→*Z1*/*Z2* isomers from LC-UV coupling for the different solvents at 40°C.

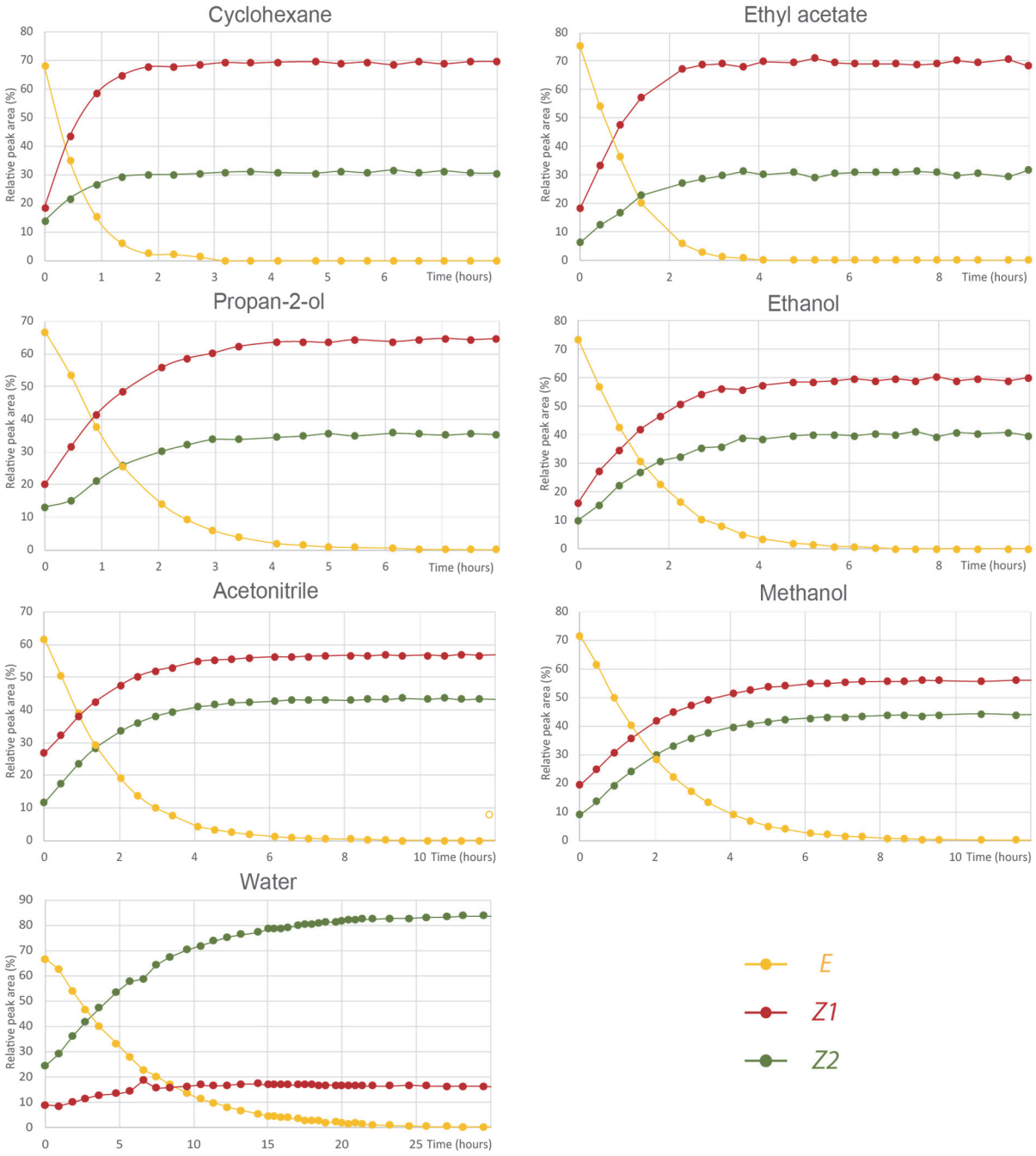

Figure S9. Plots ln[*E*] in function of the time from LC-UV experiments at 30°C.

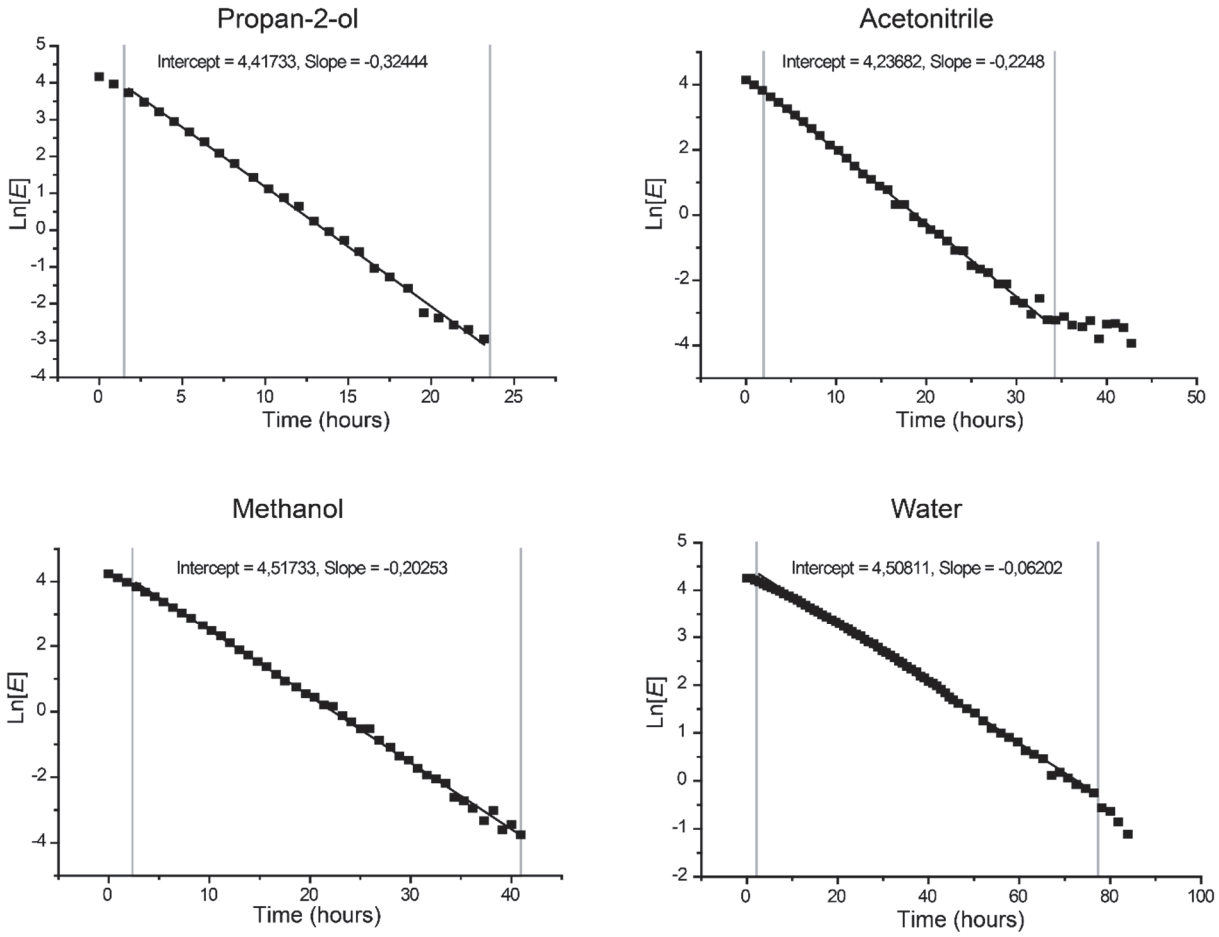

Figure S10. Plots ln[*E*] in function of the time from LC-UV experiments at 40°C.

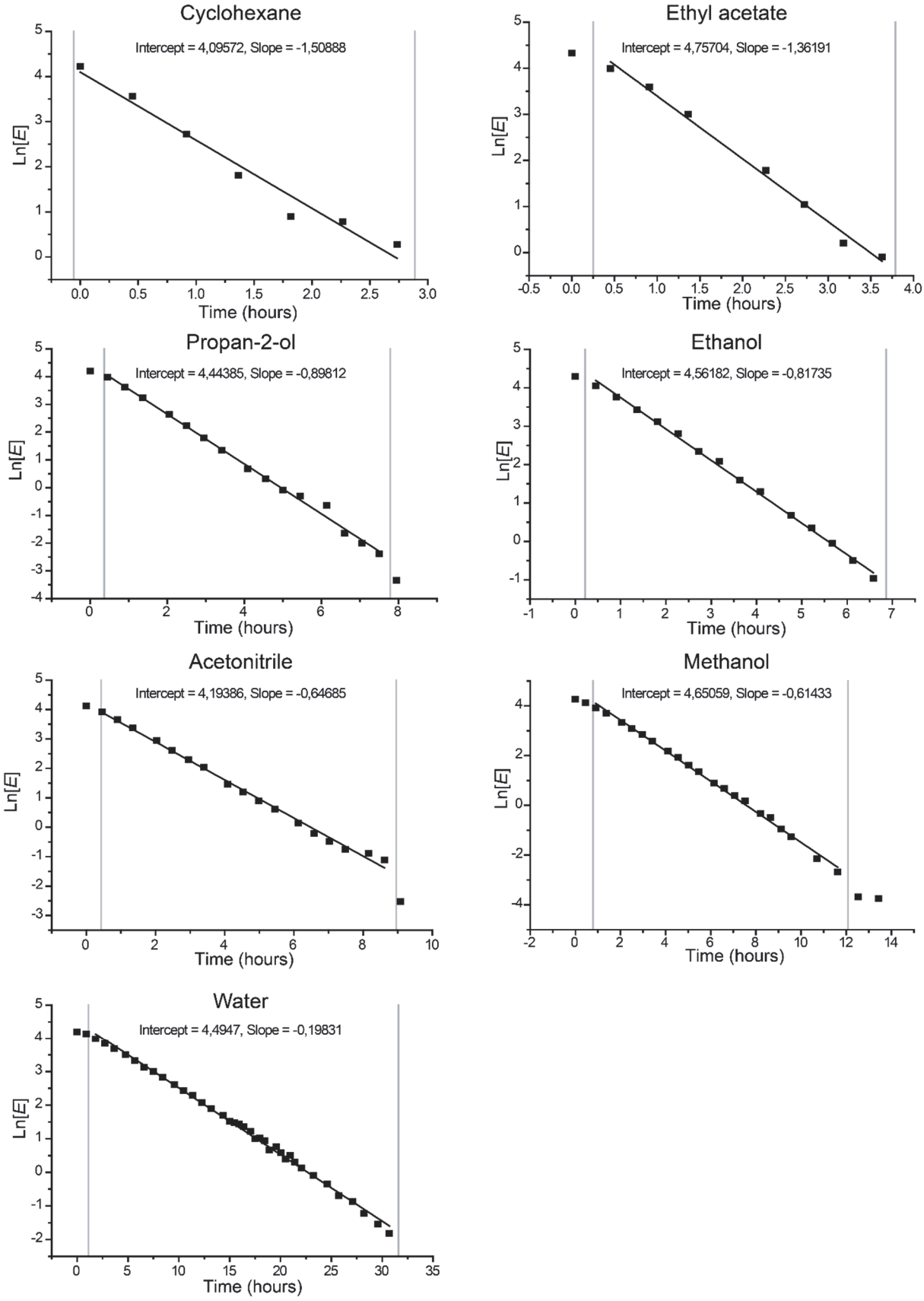

Figure S11. Extracted arrival time distributions of $[M+Ag]^+$ at *m/z* 387.0 obtained from drift tube ion mobility spectrometry after LC separation of a mixture of *Z1/Z2/E* isomers.

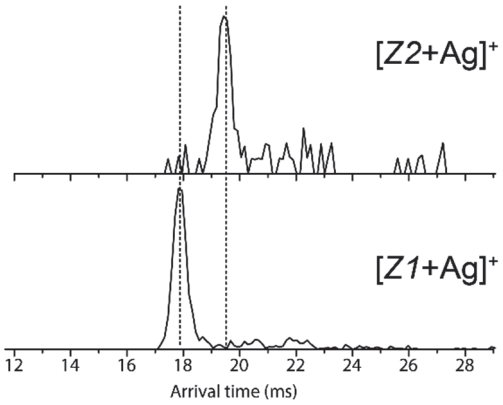

Figure S12. Extracted and fitted arrival time distributions of *m/z* 387.0 obtained from the first kinetic point of TWIMS-MS experiments at 50°C in different solvents.

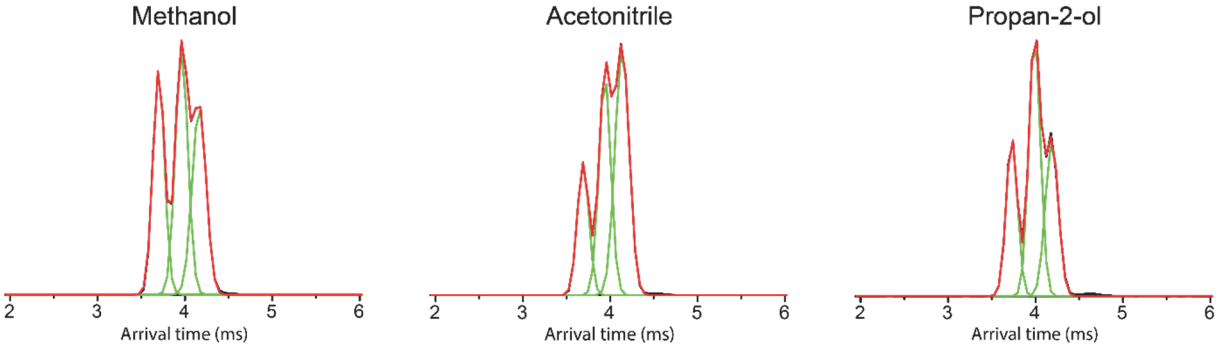

Figure S13. Structure of the various Ag^+ complexes optimized at the B3LYP/6-31G(d,p) level. Relative energies are given in kJ/mol.

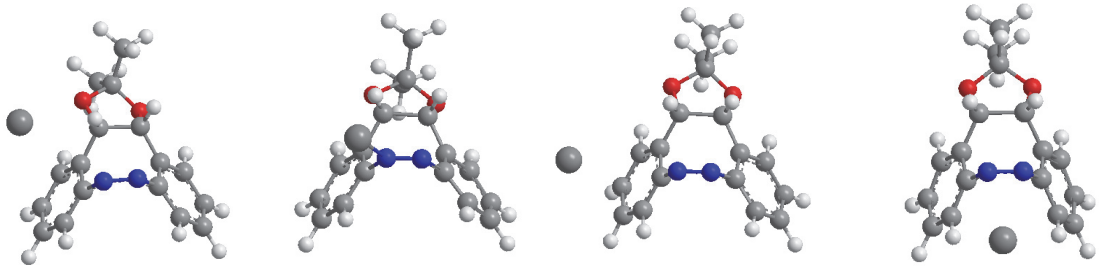

Z1_Ag1
+58.0

Z1_Ag2
26.6

Z1_Ag3
+65.4

Z1_Ag4
+20.2

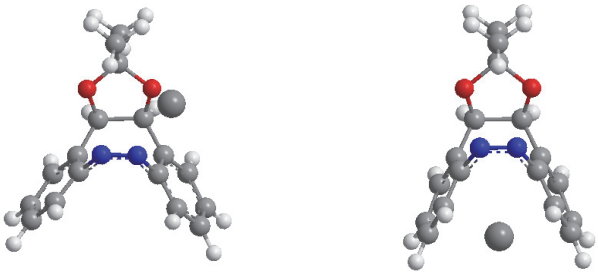

Z2_Ag1
0.0

Z2_Ag2
+37.7

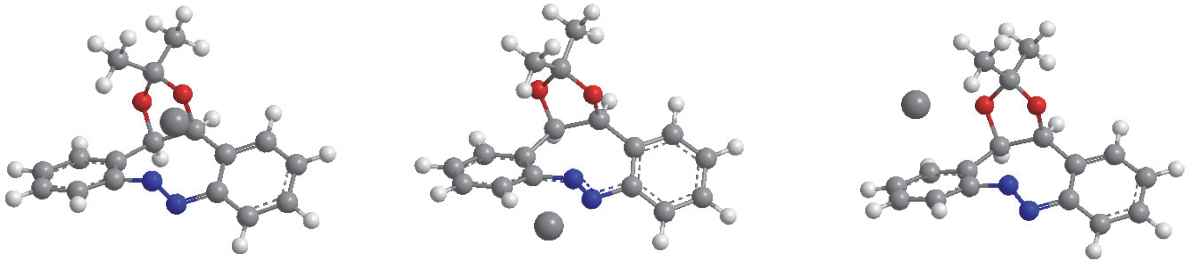

E_Ag1
+40.3

E_Ag2
+80.6

E_Ag3
+106.5

Table S2. Experimental and computed IR vibrational bands for the **Z1-Ag4** complex

Wavenumbers (cm^{-1})		DFT-computed intensities (km/mol)	Vibrational mode
Exp.	Calc.[a]		
780	763	102	γ CH benzenic
	786	30	γ CH benzenic
1042	1045	143	arom. ring breath.
1085	1089	107	ν C-O
1137	1149	20	δ C-H aro+ δ CH_3 wag.
1180	1195	198	δ CH_2 sciss. of CH_3
	1218	34	δ CH aliph.
1227	1241	58	δ CH aliph.
1349	1374	33	δ CH_3 umbrella
1398	1413	21	δ CH arom.

a) Scaled by a factor of 0.965

Table S3. Experimental and computed IR vibrational bands for the **Z2-Ag1** complex

Wavenumbers (cm^{-1})		DFT-computed intensities (km/mol)	Vibrational mode
Exp.	Calc.[a]		
748	746	61	γ CH benzenic
	755	32	γ CH benzenic
975	957	55	γ CH CH_3
1025	1019	118	ν C-O
1142	1137	57	δ CH_2 rock.
1200	1190	106	δ CH CH_3
	1203	75	δ CH arom.
1235	1244	40	δ CH CH_3
1365	1364	34	δ CH_3 umbrella

a) Scaled by a factor of 0.965

Figure S14. DFT calculated IR absorption spectrum for the optimized structures of the [*Z1*+Ag]$^{+}$ complex

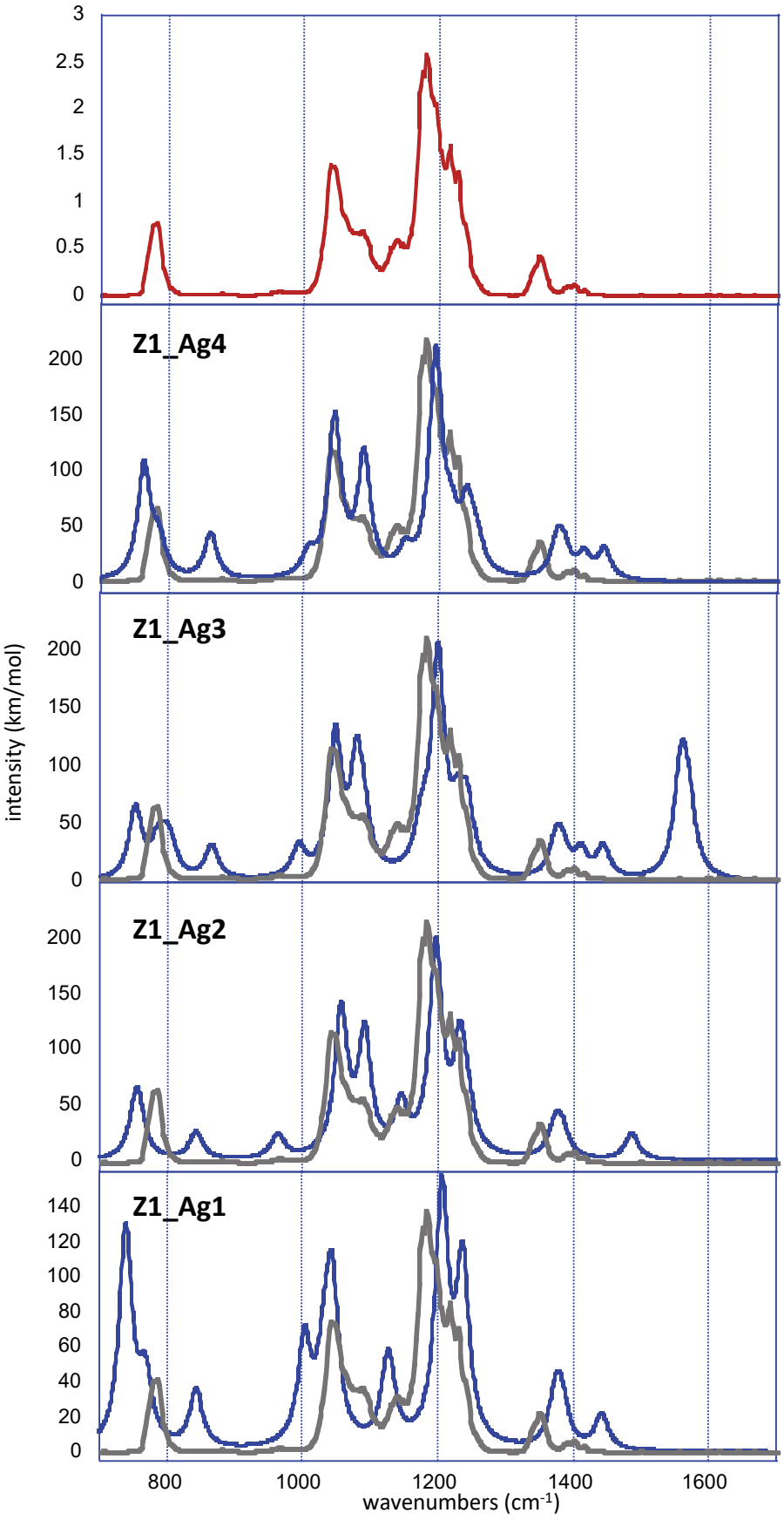

Figure S15. DFT calculated IR absorption spectrum for the optimized structures of the [*Z1*+Ag]$^+$ complex

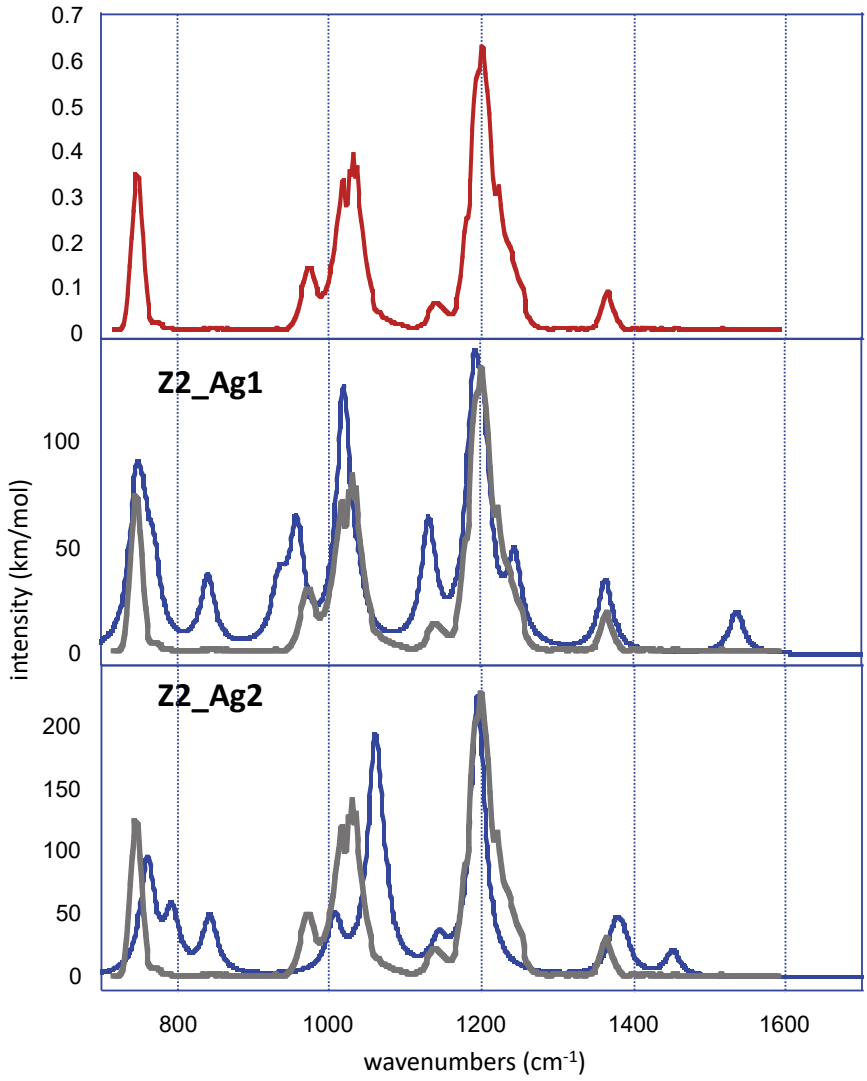

Table S4. Experimental CCS values obtained from drift tube ion mobility experiments and theoretical CCS values obtained with the TM, PA and EHSS algorithms of the MOBCAL software.

	Experimental	Theoretical		
		TM	PA	EHSS
Z1 (Z1_Ag1)	106 ± 2 Å²	101 Å²	106.9 Å²	115 Å²
Z1 (Z1_Ag2)		101.9 Å²	112.4 Å²	121.3 Å²
Z1 (Z1_Ag3)		102.5 Å²	110.4 Å²	119.4 Å²
Z1 (**Z1_Ag4**)		**96.3 Å²**	**101 Å²**	**107.2 Å²**
Z2 (**Z2_Ag1**)	115 ± 2 Å²	**97.1 Å²**	**106,4 Å²**	**114.1 Å²**
Z2 (Z2_Ag2)		115.0 Å²	93.5 Å²	100.4 Å²

Figure S16. Plots of intensities ratio of $[E+Ag]^+/[2E+Ag]^+$ in function of the time from IMS-MS experiments at 60°C.

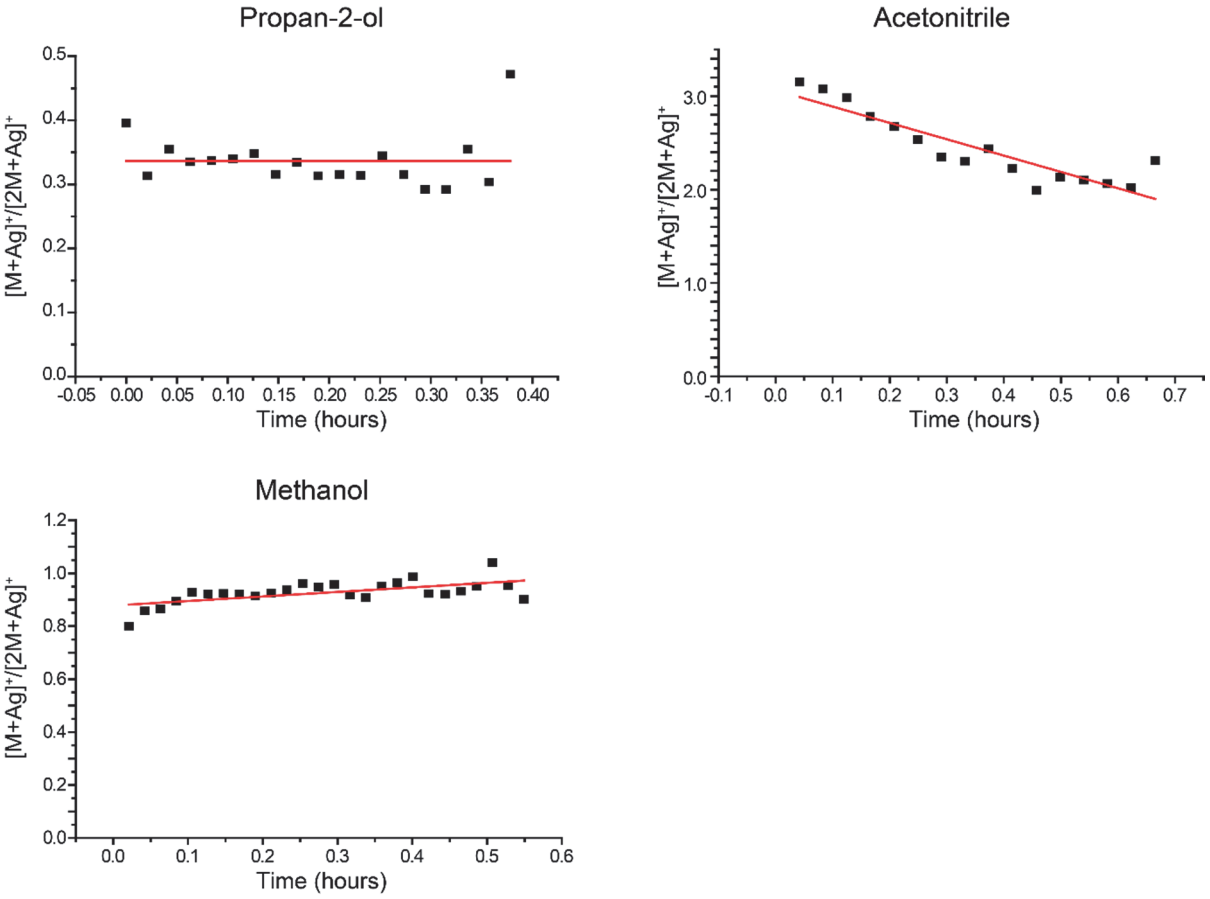

Figure S17. Plots ln[*E*] in function of the time from IMS-MS experiments at 50°C.

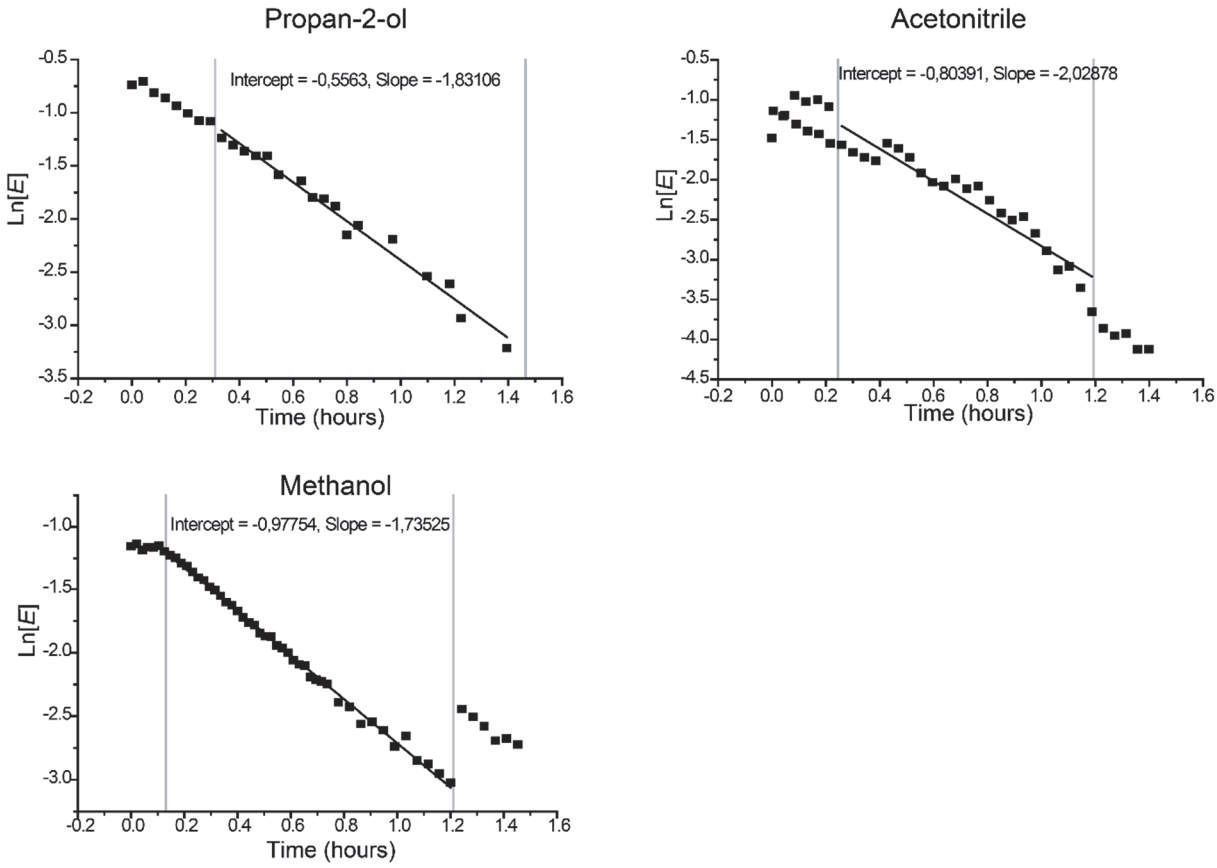

Figure S18. Plots ln[*E*] in function of the time from IMS-MS experiments at 60°C.

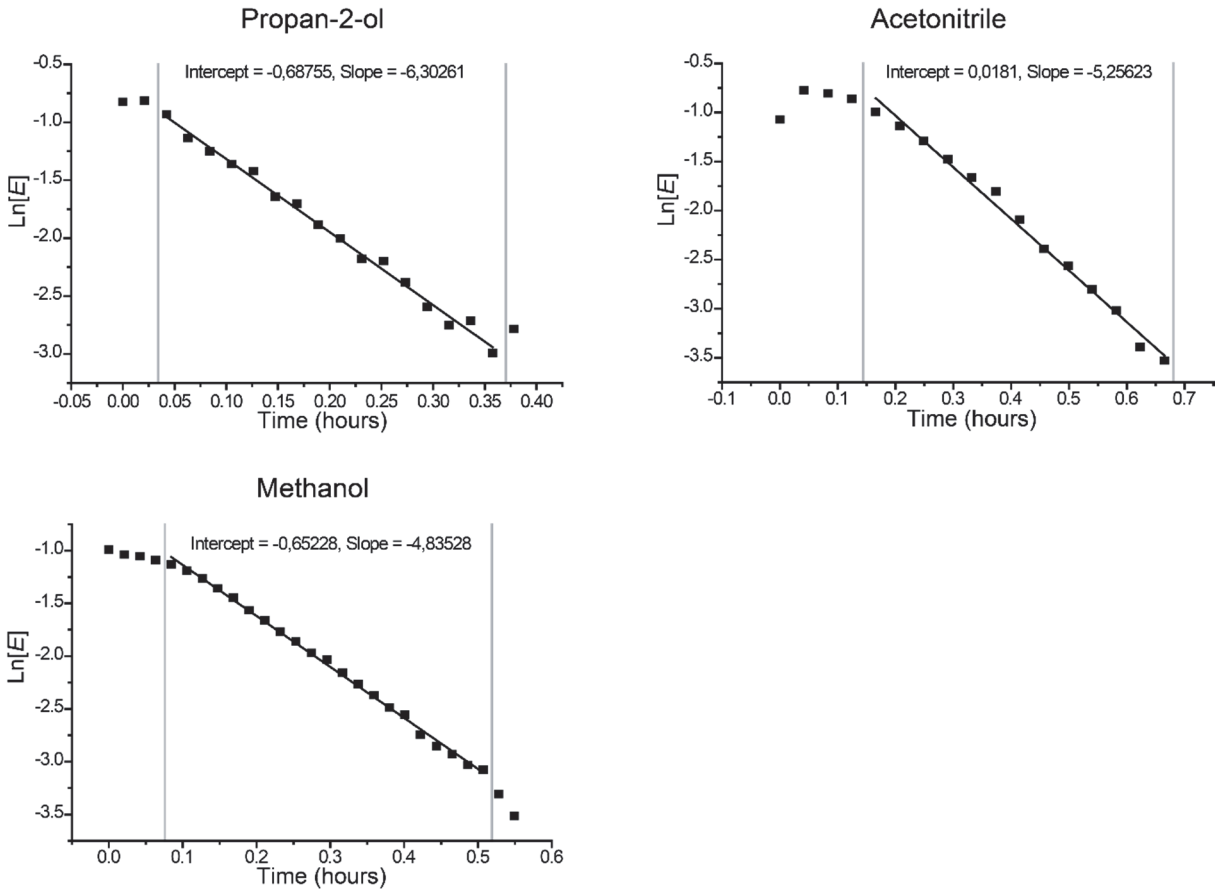

Figure S19. Plots ln[*E*] in function of the time from IMS-MS experiments at 70°C.

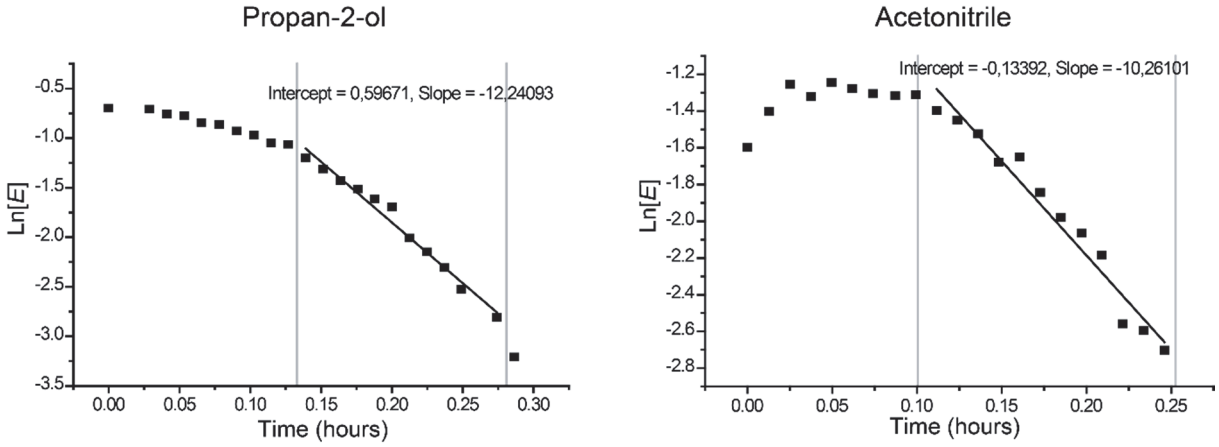

Figure S20. Plots ln[*E*] in function of the time from a) LC-UV and b) IMS-MS experiments at 40°C.

a) LC-UV experiments

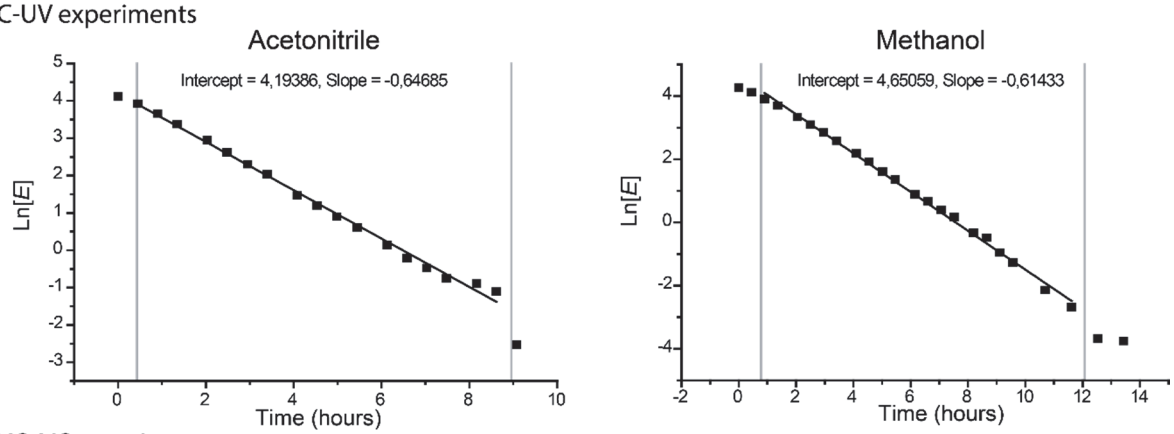

b) IMS-MS experiments